New constraints on primordial black holes abundance from femtolensing of gamma-ray bursts

A. Barnacka,[1,2,*] J.-F. Glicenstein,[2,†] and R. Moderski[1]

[1]Nicolaus Copernicus Astronomical Center, Warszawa, Poland

[2]DSM/IRFU/SPP, CEA/Saclay, F-91191 Gif-sur-Yvette, France

(Dated: April 11, 2012)

The abundance of primordial black holes is currently significantly constrained in a wide range of masses. The weakest limits are established for the small mass objects, where the small intensity of the associated physical phenomenon provides a challenge for current experiments. We used gamma-ray bursts with known redshifts detected by the Fermi Gamma-ray Burst Monitor (GBM) to search for the femtolensing effects caused by compact objects. The lack of femtolensing detection in the GBM data provides new evidence that primordial black holes in the mass range $5 \times 10^{17} - 10^{20}$ g do not constitute a major fraction of dark matter.

I. INTRODUCTION

Dark matter is one of the main and most challenging open problems in cosmology or particle physics, and a number of candidates for particle dark matter have been proposed over the years [1]. An alternative idea that the missing matter consists of compact astrophysical objects was first proposed in the 1970s [2–4]. An example of such compact objects are primordial black holes (PBHs) created in the very early Universe from matter density perturbations.

Recent advancements in experimental astrophysics, especially the launch of the FERMI satellite with its unprecedented sensitivity has revived the interest in PBH physics [5, 6]. One of the most promising way to search for PBHs is to look for lensing effects caused by these compact objects. Since the Schwarzschild radius of PBH is comparable to the photon wavelength, the wave nature of electromagnetic radiation has to be taken into account. In such a case, lensing caused by PBHs introduces an interferometry pattern in the energy spectrum of the lensed object [7]. The effect is called 'femtolensing' [8] due to very small angular distance between the lensed images. The phenomenon has been a matter of extensive studies in the past [9], but the research was almost entirely theoretical since no case of femtolensing has been detected as yet. Gould [8] first suggested that the femtolensing of gamma-ray bursts (GRBs) at cosmological distances could be used to search for dark matter objects in the mass range $10^{17} - 10^{20}$ g. Femtolensing could also be a signature of another dark matter candidate: clustered axions [10].

In this paper, we present the results of a femtolensing search performed on the spectra of GRBs with known redshifts detected by the Gamma-ray Burst Monitor (GBM) on board the FERMI satellite. The non observation of femtolensing on these bursts provides new constraints on the PBHs fraction in the mass range $5 \times 10^{17} - 10^{20}$ g. We describe in details the optical depth derivation based on simulations applied to each burst individually. The sensitivity of the GBM to the femtolensing detection is also calculated.

The paper is organized as follows: in Sec. II the basic equations for femtolensing and the calculation of lensing probability are given. Section III describes the data sample and simulations. In Sec. IV the results are presented, while Sec. V is devoted to discussion and conclusions.

II. FEMTOLENSING

A. Magnification and spectral pattern

Consider a lensing event of a GRB by a compact object. The angular diameter distances from the observer to the lens, from the lens to the GRB source and from the observer to the source are D_{OL}, D_{LS}, and D_{OS}, respectively. Coordinates are taken in the lens plane. The lens, with mass M, is located at the origin. The source position projected onto the lens plane is given by r_S, the distance between the lens and true source position. The Einstein radius r_E is given by

$$r_E^2 = \frac{4GM}{c^2}\frac{D_{OL}D_{LS}}{D_{OL}+D_{LS}} \approx (c \times 0.1\,\mathrm{s})^2 \left(\frac{4\xi - 4}{\xi^2}\right)\left(\frac{D_{OS}}{5\,\mathrm{Gpc}}\right)\left(\frac{M}{10^{19}\,\mathrm{g}}\right), \quad (1)$$

where

$$\xi = \frac{D_{OS}}{D_{OL}}\,. \quad (2)$$

The image positions are given as usual by

$$r_\pm = \frac{1}{2}(r_S \pm \sqrt{r_S^2 + 4r_E^2})\,. \quad (3)$$

The time delay δt between the two images is given by

$$c\delta t = V(r_+; r_S) - V(r_-; r_S)\,, \quad (4)$$

* e-mail: abarnack@camk.edu.pl

† e-mail: glicens@cea.fr

where $V(r; r_S)$ is the Fermat potential at the position r in the lens plane. One finds:

$$c\delta t = \frac{1}{2}\left(\frac{1}{D_{LS}} + \frac{1}{D_{OL}}\right)(r_+^2 - r_-^2) - \frac{4GM}{c^2}\ln(\frac{r_+}{r_-}) . \quad (5)$$

The phase shift between the two images is $\Delta\phi = E\,\delta t/\hbar$, where E is the energy of the photon.

In the case of a point source, the amplitude contributed by the $r_\pm$ images is

$$A_\pm \propto \frac{\exp(i\phi_\pm)}{\sqrt{|1 - \frac{r_E^4}{r_\pm^4}|}} . \quad (6)$$

The magnification A^2 is obtained by summing the amplitudes (6) and squaring, which gives

$$|A|^2 = |A_+ + A_-|^2 = \\ = \frac{1}{1 - \frac{r_E^4}{r_+^4}} + \frac{1}{1 - \frac{r_E^4}{r_-^4}} + \frac{2\cos(\Delta\phi)}{\sqrt{|1 - \frac{r_E^4}{r_+^4}|}\sqrt{|1 - \frac{r_E^4}{r_-^4}|}} . \quad (7)$$

The energy dependent magnification produces fringes in the energy spectrum of the lensed object.

In principle, the finite size of the source and the relative motion of the observer, the lens and the source have to be taken into account. If the GRB is observed at a time t_{expl} after the beginning of the burst, its size projected onto the lens plane is

$$s_{GRB} \approx \frac{D_{OL}}{D_{OS}}\frac{ct_{expl}}{\Gamma} \\ \approx (c \times 0.005\,\mathrm{s})\left(\frac{t_{expl}}{1\,\mathrm{s}}\right)\left(\frac{\Gamma}{100}\right)^{-1}\left(\frac{\xi}{2}\right)^{-1} , \quad (8)$$

where Γ is the Lorentz factor of the burst. Note that the Lorentz factor of GRBs is estimated to be in excess of 100, so that s_{GRB} given in Eq. (8) is overestimated.

The ratio of s_{GRB} to r_E is therefore

$$\frac{s_{GRB}}{r_E} \approx 0.05\,(\xi - 1)^{-\frac{1}{2}}\left(\frac{t_{expl}}{1\,\mathrm{s}}\right)\left(\frac{\Gamma}{100}\right)^{-1} \\ \times \left(\frac{D_{OS}}{5\,\mathrm{Gpc}}\right)^{-\frac{1}{2}}\left(\frac{M}{10^{19}\,\mathrm{g}}\right)^{-\frac{1}{2}} . \quad (9)$$

Equation (9) shows that the finite size of the GRB can be in general safely neglected if $t_{expl} < 10\,\mathrm{s}$.

The Einstein radius crossing time t_E is given by

$$t_E = \frac{r_E}{v} \\ \approx 100\,\mathrm{s}\left(\frac{r_E}{c \times 0.1\,\mathrm{s}}\right)\left(\frac{v}{300\,\mathrm{km/s}}\right)^{-1} , \quad (10)$$

where v is the projected velocity of the source in the lens plane. Equation (10) shows that $t_E \gg t_{expl}$ under reasonable assumptions on the velocities. If so, the motion of the source in the lens plane can also be neglected. In the analysis of GRB spectra, it is thus assumed that the point source – point lens assumption is valid and that the source stays at a fixed position in the lens plane.

B. Lensing probability

The lensing probability of gamma ray burst events is calculated in two steps. First, the optical depth τ for lensing by compact objects is calculated according to the formalism of Fukugita et al. [11]. The cosmological parameters used in the calculation are: a mean mass density $\Omega_M = 0.3$ and a normalized cosmological constant $\Omega_\Lambda = 0.7$. The calculations are made for both the Friedmann-Lematre-Robertson-Walker (FLRW) and the Dyer-Roeder [12] cosmology. In our sample, the GRB redshift z_s is known. The lens redshift z_L is assumed to be given by the maximum of the $d\tau/dz_L(z_S)$ distribution (see e.g. Fig. 5 of [11]). When $\tau \ll 1$, the lensing probability p is given by $p = \tau\sigma$ where σ is the "lensing cross-section" (see Chap. 11 of [13]).

In this paper, the cross-section is defined in the following way. Fringes are searched in the spectra of GRBs. These fringes are detectable only for certain positions r_S of the source. The exact criteria for detectability will be given in section III C. The maximum and minimum position of r_S, in units of r_E are noted $r_{S,min}$ and $r_{S,max}$. They are found by simulation and depend on the GRB redshift and luminosity. A minimum value of r_S occurs because the period of the spectral fringes becomes larger than the GBM energy range at small r_S.

The femtolensing "cross-section" is simply

$$\sigma = r_{S,max}^2 - r_{S,min}^2 \quad (11)$$

The lensing probability does not depend on the individual masses of lenses, but only on the density of compact objects Ω_{CO}. In the optical depth calculation, an increase in the mass of the lenses is compensated by a decrease in the number of scatterers. Therefore, the constraints for a given mass depend only on the cross section σ.

III. DATA ANALYSIS

In our analysis, we use a sample of GRBs with known redshifts. The selection of these bursts is described in Sec. III A. Then each burst is fitted to a standard spectral model, as explained in Sec. III B. Finally, the sensitivity of each burst to femtolensing is studied with simulated data. The simulation is described in Sec. III C.

A. Data selection

The Gamma-Ray Burst detector (GBM)[14] on-board the Fermi satellite consists of 12 NaI and 2 BGO scintillators which cover the energy range from 8 keV up to 40 MeV in 128 energy bins. These detectors perform a whole sky monitoring. In the first two years of operation, GBM triggered on roughly 500 GRBs. In this paper, only the bursts with known redshifts have been investigated. The initial sample consisted of 32 bursts taken from Gruber et al. [15] and 5 additional bursts from the GRB Coordinates Network (GCN) circulars[16].

For 17 burst the amount of available data was not sufficient to obtain good quality spectra. The final sample thus consists of 20 bursts, which are listed in the Tab. I.

B. Data processing and spectral analysis

The GBM data are publicly available in the CSPEC format and were downloaded from the Fermi FSSC website [17]. The CSPEC files contain the counts in 128 energy channels binned in 1.024 s for all detectors. Only detectors with a minimal signal to noise ratio of 5.5 in each bin were selected for the analysis.

Data were analyzed with the `RMfit` version 33pr7 program. The `RMfit` software package was originally developed for the time-resolved analysis of BATSE GRB data but has been adapted to GBM and other instruments.

For each detector with sufficient data, the background was subtracted and the counts spectrum of the first ten seconds of the burst (or less if the burst was shorter) was extracted.

The energy spectrum was obtained with a standard forward-folding algorithm. Several GRB spectral models such as a broken power law (BKN), Band's model (BAND) or a smoothly broken power law (SBKN) where considered. The femtolensing effect was added as a separate model. The magnification and the oscillating fridges where calculated according to Eq. (7), then multiplied with the BKN or BAND functions.

C. Simulations

The detectability of spectral fringes has been studied with simulated signals. The detectability depends on one side on the luminosity and the redshift of the bursts, and on the other side on the detector energy resolution and the data quality. The sensitivity of the GBM to the lens mass M depends strongly also on the energy range and resolution of the GBM detectors. When small masses are considered, the pattern of spectral fringes appears outside of the energy range. The large masses produce fringes with hardly detectable amplitudes and periods smaller than the energy bin size.

Because the data quality and the background are not easily simulated, the detectability estimation is performed on real data. Namely, GRB events with known redshift are selected. Since the source redshift is known, the lens redshift is assumed to be the maximum value of $d\tau/dz_L(z_S)$ as explained in Sec. II B. For a given observed GRB, the femtolensing signal depends thus only on 2 parameters: the lens mass M and the source position in the lens plane r_S. The data are then processed as follows:

1. The magnification (Eq. 7) as a function of the energy is calculated for the given lens mass M and position of the source r_S.

2. This magnification is then convolved with the instrumental resolution matrix to obtain magnification factors for each channel of the detector.

3. The spectral signal is extracted from the data by subtracting the background. It is then multiplied by the corrected magnification.

4. The background is added back.

The detectability calculation can be illustrated with the luminous burst GRB090424592. The spectral data of this burst were first fitted with standard spectral models: BKN, SBKN and BAND. The GRB090424952 burst is best fitted with the BAND model. The fit has $\chi^2 = 78$ for 67 degrees of freedom (d.o.f). The BAND model has 4 free parameters: the amplitude A, the low energy spectral index α, the high energy spectral index β and the peak energy E_{peak} [18].

The data are then modified by incorporating the spectral fringe patterns for a range of lens masses M and source positions r_S. The simulated data and the corresponding femtolensing fit are presented in Fig. 1. Neither BKN nor BAND models are able to fit the simulated data (see Fig. 2). The values of r_S are then changed until the χ^2 of the fit obtained is not significantly different from the χ^2 of the unmodified data. More precisely, the χ^2 difference $\Delta\chi^2$ should be distributed in the large sample limit as a χ^2 distribution with 2 degrees of freedom according to Wilk's theorem [19]. The value $\Delta\chi^2 = 5.99$, which corresponds to a χ^2 probability of 5% for 2 d.o.f, was taken as the cut value. The effect of changing r_S on the femtolensing model is illustrated on Fig. 3 and 4.

In Fig. 5 we show the maximum and minimum detectable r_S for different lens masses. The maximum difference between $r_{S,max}$ and $r_{S,min}$ appears at $M = 5 \times 10^{18}$ g, which indicates the maximum of femtolensing cross-section.

IV. RESULTS

The 20 burst sample from Tab. I have been fitted with the standard BKN, BAND and SBKN models. The models with the best χ^2 probability were selected and are shown on Tab. I. The bursts are well fitted by these standard models, so that there is no evidence for femtolensing in the data.

As explained in section II B, the lensing probability for each burst depends on the lens mass and on the $r_{S,min}$ and $r_{S,max}$ values. Since the sensitivity of GBM to femtolensing is maximal for lens masses of $\sim 5 \times 10^{18}$ g (see Fig. 5), the values of $r_{S,min}$ and $r_{S,max}$ for each event were first determined at a mass $M = 5 \times 10^{18}$ g by simulation. As explained in Sec. II B, the value of

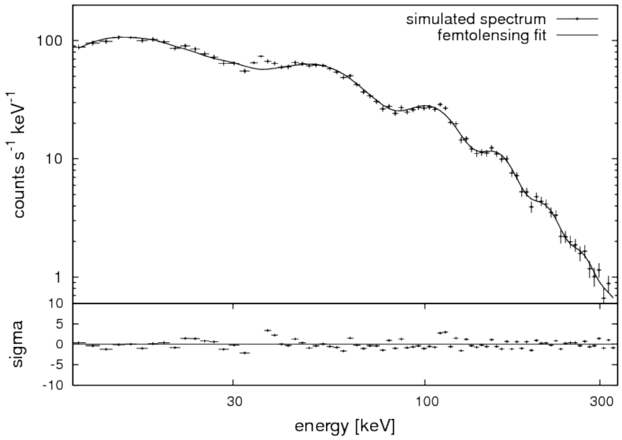

FIG. 1. Simulated spectrum obtained with GRB 090424592. The spectrum was fitted with femtolensing+BAND model. The fit has $\chi^2 = 92$ for 73 d.o.f. The fit parameters are: $A = 0.34 \pm 0.02\,\mathrm{ph\,s^{-1}\,cm^{-2}\,keV^{-1}}$, $E_{peak} = 173 \pm 12\,\mathrm{keV}$, $\alpha = -0.84 \pm 0.03$ and $\beta = -3.9 \pm 7.5$. The simulated femtolensing effect is caused by a lens at redshifts $z_L = 0.256$ and a source at $z_S = 0.544$. The simulated mass is $M = 5 \times 10^{18}$ g and the mass reconstructed from the fit is 5.8×10^{18} g. The source is simulated at position $r_S = 2$. The position reconstructed from the fit is $r_S = 1.9$.

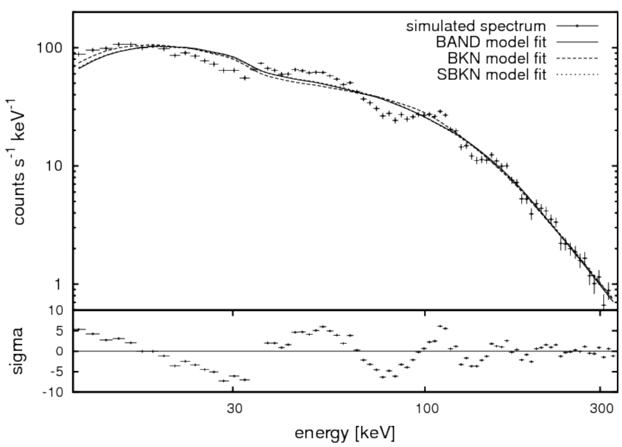

FIG. 2. Simulated femtolensed spectrum fitted with the BAND model. The fit has $\chi^2 = 810$ for 75 d.o.f. The fit parameters are: $A = 0.5 \pm 0.03\,\mathrm{ph\,s^{-1}\,cm^{-2}\,keV^{-1}}$, $E_{peak} = 147 \pm 5\,\mathrm{keV}$, $\alpha = -0.58 \pm 0.03$ and $\beta = -2.4 \pm 0.1$. The SBKN model fit is almost indistinguishable from the BKN model fit.

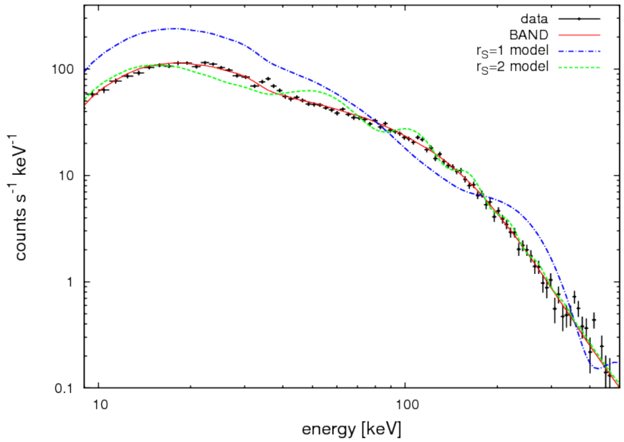

FIG. 3. The spectrum of GRB 090424592 using NaI detector n7, with the BAND and femtolensing fits superimposed. The parameters are $r_S = 1,\ 2$, and lens mass 5×10^{18} g. The models are convolved with the response matrix.

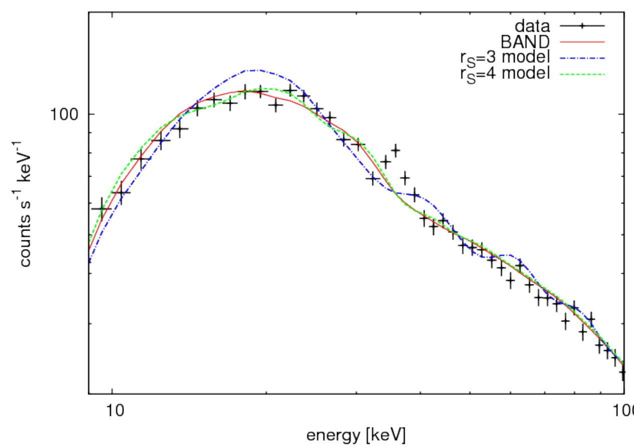

FIG. 4. The spectrum of GRB 090424592 using NaI detector n7. The BAND and femtolensing fits are superimposed. The parameters are $r_S = 3,\ 4$, and lens mass 5×10^{18} g. The excess at 33 keV (K-edge) is an instrumental effect seen on many bright bursts.

$r_{S,min}$ is set by the period of the spectral fringes so that it is independent of the burst luminosity. The values of $r_{S,max}$ obtained are listed in Tab. I. The lensing probability is then calculated for both the FRLW and Dyer & Roeder cosmological models using each burst redshift, the most probable lens position and the values of $r_{S,min}$ and $r_{S,max}$ for the mass $M = 5 \times 10^{18}$ g. The number of expected lensed bursts in the sample is the sum of the lensing probabilities. It depends linearly on Ω_{CO}.

Since no femtolensing is observed, the number of expected events should be less than 3 at 95% confidence level (C.L.). The constraints on the density of compact objects Ω_{CO} is derived to be less than 4% at 95% C.L for both cosmological models. The values of the lensing probabilities for all the bursts in our sample assuming the constrained density of compact objects are shown in Tab. I. The limits at other lens masses are obtained by normalizing the Ω_{CO} at $M = 5 \times 10^{18}$g by the cross section σ. The cross section is calculated using the Eq. 11 and the values of $r_{S,min}$ and $r_{S,max}$ from Fig. 5. The limits on Ω_{CO} at 95% C.L. are plotted in Fig. 6.

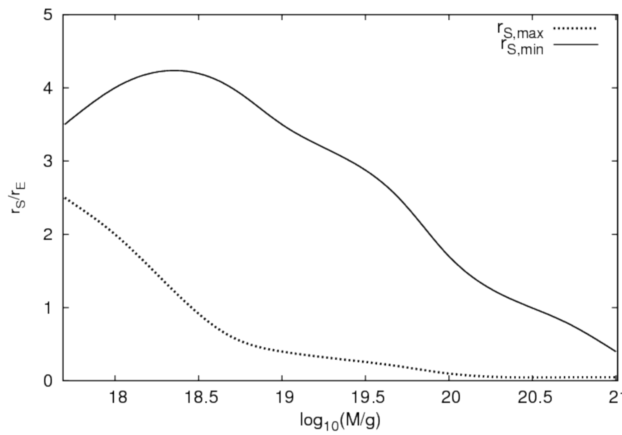

FIG. 5. Minimum and maximum detectable r_S/r_E as a function of lens mass for GRB 090424592.

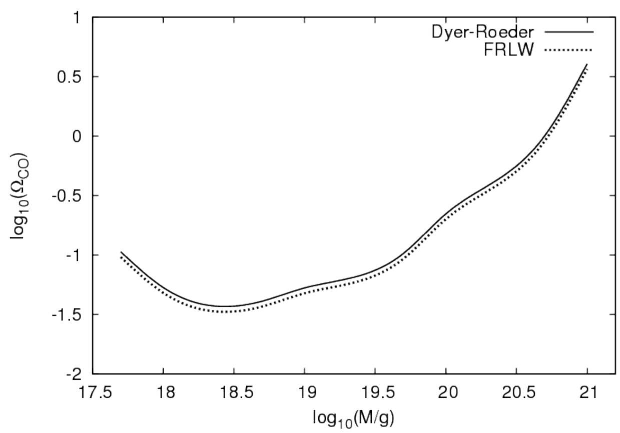

FIG. 6. Constraints on the fraction (or normalize density) of compact objects. The zones above the curves are excluded at the 95% confidence level.

V. DISCUSSION AND CONCLUSIONS

Cosmological constraints on the PBH abundance are reviewed by Carr et al. [5]. One way to obtain the abundance of PBH is to constrain the density of compact objects Ω_{CO}. Note that the limits on the compact object abundance in the $10^{26} - 10^{34}$ g range obtained with microlensing are at the 1% level.

It is stated in Abramowicz et al. [20] that the mass range $10^{16}\,\mathrm{g} < M_{BH} < 10^{26}\,\mathrm{g}$ is virtually unconstrained. Under this range, the Ω_{CO} is constrained by PBH evaporation. Above this range, the constraints come from microlensing. The new idea by Griest et al. [6] shows that the microlensing limit could be improved and get constraints down to 10^{20} g with the Kepler satellite observations.

The FERMI satellite was launched three and a half years ago. Since then, almost 1000 of GRB were observed with the GBM detector. In many cases data quality is good enough to reconstruct time-resolved spectra. This unique feature is exploited in our femtolensing search by selecting the first few seconds of a burst in data analysis.

Our limits were obtained by selecting only those bursts with known redshifts in the GBM data. This reduces the data sample from the 500 bursts detected in the first 2 years to only 20. The constraints on Ω_{CO} obtained at the 95% C.L. are shown on Fig. 6. These constraints improve the existing constraints by a factor of 4 in the mass range $5 \times 10^{17} - 10^{20}$ g.

After ten years of operation, the GBM detector should collect over 2500 bursts. Only a few of the bursts, say 100, will have a measured redshift and sufficient spectral coverage. By applying the methods described in this paper, our limits will then improve by a factor of 5 reaching a sensitivity to density of compact objects down to the 1% level.

ACKNOWLEDGMENTS

Part of this research was supported by the Polish Ministry of Science and Higher Education under grant no. DEC-2011/01/N/ST9/06007 and grant no. ERA-NET-ASPERA/01/10.

[1] J. L. Feng, Annual Review of Astronomy and Astrophysics **48**, 495 (2010), http://www.annualreviews.org/doi/pdf/10.1146/annurev-astro-082708-101659.
[2] B. J. Carr and S. W. Hawking, Mon. Not. R. Astron. Soc. **168**, 399 (1974).
[3] S. W. Hawking, Nature (London) **248**, 30 (1974).
[4] S. Hawking, Mon. Not. R. Astron. Soc. **152**, 75 (1971).
[5] B. J. Carr, K. Kohri, Y. Sendouda, and J. Yokoyama, Phys. Rev. D **81**, 104019 (2010), arXiv:0912.5297 [astro-ph.CO].
[6] K. Griest, M. J. Lehner, A. M. Cieplak, and B. Jain, Phys. Rev. Lett. **107**, 231101 (2011), arXiv:1109.4975 [astro-ph.CO].
[7] A. V. Mandzhos, Sov. Astron. Lett. **7**, 213 (1981).
[8] A. Gould, Astrophys. J. **386**, L5 (1992).
[9] A. Gould, in *Microlensing 2000: A New Era of Microlensing Astrophysics*, Astronomical Society of the Pacific Conference Series, Vol. 239, edited by J. W. Menzies & P. D. Sackett (2001) p. 3, arXiv:astro-ph/0004042.
[10] E. W. Kolb and I. I. Tkachev, Astrophys. J. Lett. **460**, L25 (1996), arXiv:astro-ph/9510043.
[11] M. Fukugita, T. Futamase, M. Kasai, and E. L. Turner, Astrophys. J. **393**, 3 (1992).
[12] C. C. Dyer and R. C. Roeder, Astrophys. J. **180**, L31 (1973).

[13] P. Schneider, J. Ehlers, and E. E. Falco, *Gravitational Lenses, XIV, 560 pp. 112 figs.. Springer-Verlag Berlin Heidelberg New York. Also Astronomy and Astrophysics Library* (Springer-Verlag Berlin Heidelberg New York, 1992).

[14] C. Meegan, G. Lichti, P. N. Bhat, E. Bissaldi, M. S. Briggs, V. Connaughton, R. Diehl, G. Fishman, J. Greiner, A. S. Hoover, A. J. van der Horst, A. von Kienlin, R. M. Kippen, C. Kouveliotou, S. McBreen, W. S. Paciesas, R. Preece, H. Steinle, M. S. Wallace, R. B. Wilson, and C. Wilson-Hodge, Astrophys. J. **702**, 791 (2009), arXiv:0908.0450 [astro-ph.IM].

[15] D. Gruber, J. Greiner, A. von Kienlin, A. Rau, M. S. Briggs, V. Connaughton, A. Goldstein, A. J. van der Horst, M. Nardini, P. N. Bhat, E. Bissaldi, J. M. Burgess, V. L. Chaplin, R. Diehl, G. J. Fishman, G. Fitzpatrick, S. Foley, M. H. Gibby, M. M. Giles, S. Guiriec, R. M. Kippen, C. Kouveliotou, L. Lin, S. McBreen, C. A. Meegan, F. Olivares E., W. S. Paciesas, R. D. Preece, D. Tierney, and C. Wilson-Hodge, Astron. Astrophys. **531**, A20 (2011), arXiv:1104.5495 [astro-ph.HE].

[16] Http://gcn.gsfc.nasa.gov.

[17] Http://fermi.gsfc.nasa.gov/ssc/.

[18] A. Goldstein, J. M. Burgess, R. D. Preece, M. S. Briggs, S. Guiriec, A. J. van der Horst, V. Connaughton, C. A. Wilson-Hodge, W. S. Paciesas, C. A. Meegan, A. von Kienlin, P. Narayana Bhat, E. Bissaldi, V. Chaplin, R. Diehl, G. J. Fishman, G. Fitzpatrick, S. Foley, M. Gibby, M. Giles, J. Greiner, D. Gruber, R. M. Kippen, C. Kouveliotou, S. McBreen, S. McGlynn, A. Rau, and D. Tierney, ArXiv e-prints (2012), arXiv:1201.2981 [astro-ph.HE].

[19] J. R. Mattox, D. L. Bertsch, J. Chiang, B. L. Dingus, S. W. Digel, J. A. Esposito, J. M. Fierro, R. C. Hartman, S. D. Hunter, G. Kanbach, D. A. Kniffen, Y. C. Lin, D. J. Macomb, H. A. Mayer-Hasselwander, P. F. Michelson, C. von Montigny, R. Mukherjee, P. L. Nolan, P. V. Ramanamurthy, E. Schneid, P. Sreekumar, D. J. Thompson, and T. D. Willis, Astrophys. J. **461**, 396 (1996).

[20] M. A. Abramowicz, J. K. Becker, P. L. Biermann, A. Garzilli, F. Johansson, and L. Qian, Astrophys. J. **705**, 659 (2009), arXiv:0810.3140.

[21] G. F. Marani, R. J. Nemiroff, J. P. Norris, K. Hurley, and J. T. Bonnell, Astrophys. J. Lett. **512**, L13 (1999), arXiv:astro-ph/9810391.

[22] M. S. Briggs, D. L. Band, R. D. Preece, G. N. Pendleton, W. S. Paciesas, and J. L. Matteson, in *Gamma-Ray Bursts, 4th Hunstville Symposium*, American Institute of Physics Conference Series, Vol. 428, edited by C. A. Meegan, R. D. Preece, & T. M. Koshut (1998) pp. 299–303, arXiv:astro-ph/9712096.

TABLE I. The sample of 20 GBM GRBs used in the analysis.

Name	z_S	Fit to the data [a]		Fit to simulated data		$r_{S,max}$	z_L	Lensing Probability	
		Model	χ^2/d.o.f	Model χ^2/d.o.f	Femtolensing χ^2/d.o.f			FRLW [b]	Dyer-Roeder [c]
GBM 080804972	2.2045	BAND	68/74	116/63	65/61	2	0.770	0.110	0.112
GBM 080916009C	4.3500	BKN	68/75	91/86	78/84	3	1.087	0.580	0.539
GBM 080916406A	0.6890	BKN	58/57	122/87	110/85	3	0.324	0.036	0.040
GBM 081121858	2.5120	BKN	39/49	52/49	42/47	3	0.829	0.296	0.298
GRB 081222204	2.7000	BKN	73/66	82/62	63/60	3	0.859	0.326	0.325
GRB 090102122	1.5470	BAND	81/85	103/85	93/83	3	0.603	0.146	0.154
GRB 090323002	3.5700	BAND	77/77	121/64	90/62	2	0.964	0.206	0.197
GRB 090328401	0.7360	BKN	105/70	123/70	103/68	2	0.346	0.018	0.020
GRB 090424592	0.5440	BAND	78/67	115/75	97/73	4	0.256	0.042	0.046
GRB 090510016	0.9030	BKN	62/66	173/98	158/96	1.5	0.406	0.015	0.016
GRB 090618353	0.5400	BAND	59/72	79.5/72	66/70	3	0.254	0.023	0.025
GRB 090926181	2.1062	BAND	87/81	105/81	93/79	4	0.737	0.413	0.423
GRB 091003191	0.8969	BKN	93/94	105/94	94/92	3	0.400	0.059	0.064
GRB 091020900	1.7100	BKN	74/69	116/69	90/67	2.5	0.667	0.119	0.124
GRB 091127976	0.4900	BAND	78/74	84/74	76/72	4	0.240	0.034	0.037
GRB 091208410	1.0630	BAND	55/55	115/59	56/57	2.5	0.457	0.055	0.059
GRB 100414097	1.3680	BKN	65/61	97.5/68	86/66	2.5	0.560	0.084	0.089
GRB 100814160A	1.4400	BKN	42/40	138/42	128/40	2	0.590	0.058	0.061
GRB 100816009	0.8049	BKN	73/52	95/50	66/48	2.5	0.360	0.034	0.037
GRB 110731465	2.8300	SBKN	72/64	125/64	97/62	3	0.877	0.347	0.344

[a] Fit has been performed using only the photons arrived in less than 10s from the beginning of the burst.
[b] for assumed $\Omega_{CO} = 0.037$
[c] for assumed $\Omega_{CO} = 0.041$